J. Cent. South Univ. (2021) 28: 2724−2734
DOI: https://doi.org/10.1007/s11771-021-4804-9

Springer

Synchronous enrichment of phosphorus and iron from a high-phosphorus oolitic hematite ore to prepare Fe-P alloy by direct reduction-magnetic separation process

LI Si-wei(李思唯), PAN Jian(潘建), ZHU De-qing(朱德庆), YANG Cong-cong(杨聪聪)*, GUO Zheng-qi(郭正启), DONG Tao(董韬), LU Sheng-hu(鲁胜虎)

School of Mineral Processing and Bioengineering, Central South University, Changsha 410083, China

Abstract: In this study, direct reduction-magnetic separation process was applied to enrich phosphorus and iron to prepare Fe-P crude alloy from a high phosphorus oolitic hematite ore (HPOH). The results show that at lower temperatures and with absence of any of additives, Fe cannot be effectively recovered because of the oolitic structure is not destroyed. In contrast, under the conditions of 15% Na_2SO_4 and reducing at 1050 °C for 120 min with a total C/Fe ratio (molar ratio) of 8.5, a final Fe-P alloy containing 92.40% Fe and 1.09% P can be obtained at an overall iron recovery of 95.43% and phosphorus recovery of 68.98%, respectively. This metallized Fe-P powder can be applied as the burden for production of weathering resistant steels. The developed process can provide an alternative for effective and green utilization of high phosphorus iron ore.

Key words: high-phosphorus oolitic hematite ore; direct reduction; magnetic separation; Fe-P alloy

Cite this article as: LI Si-wei, PAN Jian, ZHU De-qing, YANG Cong-cong, GUO Zheng-qi, DONG Tao, LU Sheng-hu. Synchronous enrichment of phosphorus and iron from a high-phosphorusoolitic hematite ore to prepare Fe-P alloy by directreduction-magnetic separation process [J]. Journal of Central South University, 2021, 28(9): 2724−2734. DOI: https://doi.org/10.1007/s11771-021-4804-9.

1 Introduction

Weathering steels (WSs) mainly contain low carbon and other alloying elements (Cu, Cr, Ni, P, etc.) with a total content ranging from 1.00 wt% to 5.00 wt% [1]. Due to the presence of various alloying elements, WS could provide optimum balance of corrosion resistance and strength [2, 3]. Therefore, WSs are widely used as raw materials for building bridges, load-bearing structures, and transmission towers, etc. [4]. Phosphorus is one of the crucial elements in these steels to improve corrosion resistance and ductility [5]. In weathering steel-making process, phosphorus-bearing material (such as Fe-P alloy and phosphosiderite) is added to adjust P content of WSs, resulting in its high production cost [6].

High-phosphorus oolitic hematite (HPOH) ore is abundantly found in France, America, Canada, and China, which contains several metals, indicating that it has a high comprehensive utilization value [7−9]. Generally, it contains 0.1%−1.5% P and 35%−50% Fe, and the phosphorus and iron mainly

Foundation item: Projects(AA18242003, AA148242003) supported by Innovation-driven Project of Guangxi Zhuang Autonomous Region, China; Project(51474161) supported by the National Natural Science Foundation of China
Received date: 2020-11-11; **Accepted date:** 2021-03-03
Corresponding author: YANG Cong-cong, PhD, Lecturer; Tel: +86-15874282535; E-mail: smartyoung@csu.edu.cn; ORCID: http://orcid.org/0000-0001-8609-9643

exist in the form of apatite and hematite. Moreover, oolitic hematite ores are composed of ooids with concentric layers of alternate iron minerals and gangue minerals [10]. Thus, it is significantly difficult to separate Fe and P from HPOH ore.

Direct reduction-magnetic separation (DRMS) is widely used to upgrade iron and remove phosphorus from complicate iron ores [11−14]. In recent years, many researches have been adopted to manufacture metallic iron powder from HPOH by DRMS process [15−20].

During reduction of HPOH the ore, the dephosphorization efficiency is low in the absence of additive, resulting in the metallic iron containing a high P content. TANG et al [18] adopted gas-based reduction to treat a high phosphorus (1.2%) hematite ore at 800 °C for 5 h without additive. The results showed that there was 0.27% phosphorus in the metal sample, which mainly existed in the form of apatite, resulting in the fact that it could not be removed. Similar conclusions have been reported in previous investigations [21, 22]. Therefore, additives (such as sodium salt, and calcium salt) or high temperature reduction without additive were used to enhance the dephosphorization [23 − 25]. RAO et al [23] roasted the oolitic iron ore at 1050 °C with 20% Na_2SO_4, and found that the phosphorus content in the metallic phase was 0.02% and most of the phosphorus entered the gangue phase as calcium phosphate. Without prior dephosphorizing, an innovative method was proposed to synchronous-enriched phosphorus and iron to prepare Fe-P alloy from HPOH ore [26−28]. In reduction, phosphorus existed in the form of Fe_3P in the metallic iron phase, and then the metallic iron was recovered by magnetic separation. The magnetic separation concentrate can be directly used as a burden for weather resistant steel [26].

In this paper, Fe-P alloy was prepared from HPOH by reduction at low temperature with additive. The effects of reduction parameters, carbon-burdened and Na_2SO_4 on the behavior of iron and phosphorus were investigated. The mechanisms of carbon-burden and Na_2SO_4 on the distribution of Fe and P were investigated.

2 Materials and methods

2.1 Materials

2.1.1 High-phosphorus oolitic hematite ore

Table 1 shows the chemical compositions of the hematite ore. The main ingredient of the ore is 41.50% Fe_{total}, and the content of P also reached 1.24%, which is much higher than the quality requirements of burdens for blast furnace. The X-ray diffraction (XRD) spectrum of iron ore is shown in Figure 1, which indicates that the main mineral phases in the ore are hematite (Fe_2O_3), chlorite ($Fe_3Si_2O_5(OH)_4$), fluorapatite ($Ca_5(PO_4)_3F$), kaolinite ($Al_2Si_2O_5(OH)_4$) and quartz (SiO_2). Tables 2 and 3 present the distribution characteristics of iron and phosphorous in mineral phases in the HPOH ore. Iron mainly exists in the

Table 1 Main chemical compositions of HPOH ore (wt%)

TFe	P	SiO_2	Al_2O_3	CaO	MgO	S	LOI
41.50	1.24	17.04	4.68	7.82	1.54	0.09	5.72

Note: LOI−Loss on ignition.

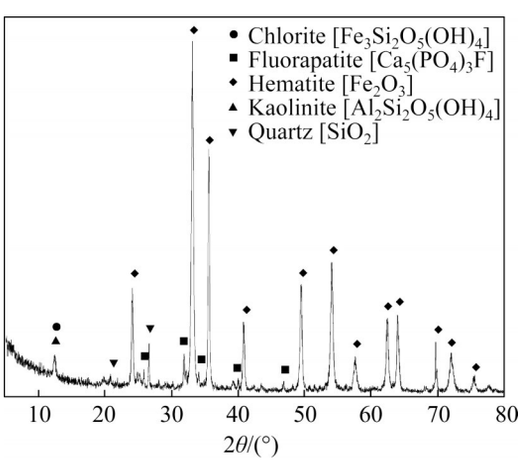

Figure 1 XRD pattern of HPOH ore

Table 2 Distribution of iron in mineral phases in HPOH ore (wt%)

Hematite	Magnetic	Fayalite	Iron carbonate	Iron sulfide	Total iron
96.69	1.83	1.36	0.07	0.05	100

Table 3 Distribution of phosphorus in mineral phase in HPOH ore (wt%)

Apatite	Iron phosphate	Others	Total P
94.76	3.31	1.94	100.00

form of hematite, and phosphorus mainly exists in the form of apatite.

Scanning electron microscope (SEM) and EDAX 32 genesis spectrometer (EDS) were used to observe the microstructure of raw ore and the results are shown in Figure 2. Table 4 presents the element content of points 1−6 in Figure 2. Hematite contains a small amount of phosphorus, which is attributed to ion absorption, isomorphism of phosphorus in the hematite (Points 1 − 4). The phosphorus at point 5 exists in the form of apatite. The chlorite contains calcium and phosphorus, but the content of phosphorus is higher than calcium, indicating that the phosphorus exists in the form of apatite in chlorite, and it exists in the form of ion absorption.

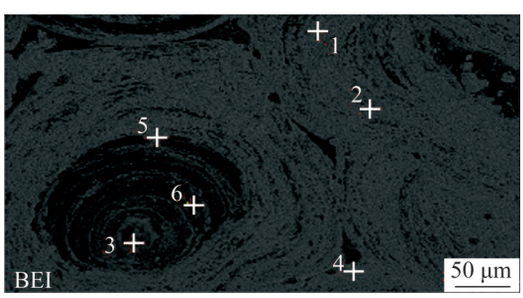

Figure 2 SEM image of in HPOH ore

Table 4 Element content (wt%) of points 1−6 in Figure 2

Point	O	Mg	Al	Si	P	Ca	Fe
1	24.44	–	1.03	0.84	0.24	nd	73.45
2	25.85	nd	1.02	0.88	0.18	0.01	72.05
3	26.68	nd	3.42	1.85	0.80	0.07	67.18
4	24.61	nd	1.38	1.03	0.32	0.04	72.62
5	19.85	nd	1.18	1.35	18.63	48.25	10.74
6	37.81	1.68	13.94	15.78	0.35	0.23	30.20

Note: nd–below detection limit.

The TG-DSC curve of HPOH is presented in Figure 3. It can be seen from the TG curve of raw ore that the quality of the sample decreases with increasing temperature, and there are two weight loss processes. Due to the decomposition of siderite between 25 and 463 °C, the weight loss rate is 5.39%. The second stage ranges from 463 to 1271 °C, which is caused by the defluorination reaction between quartz and fluorapatite in the ore [29].

In order to find whether or not phosphorus exists in the form of ion absorption in the oolitic hematite, the following two groups of analytical

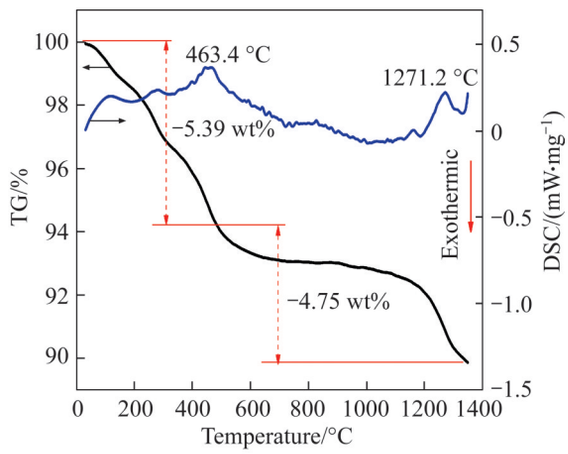

Figure 3 TG-DSC curve of HPOH ore

tests (distilled water and 10% Na_2SO_4) were carried out. The results show that the dissolutions of two groups are 1.94% and 2.50%, respectively, confirming that there is a small amount of phosphorus in the form of ion absorption.

Soft coal was used as a reductant in this study. The soft coal contains 52.63% fixed carbon, 5.31% ash and 35.15% volatile matter (mass fraction). The softening temperature of ash is 1244 °C, indicating that it is a superior reducing agent [30].

2.1.2 Additive

Analytically pure Na_2SO_4 was used as additive in this study to promote the reduction of fluorapatite. Its particle size is below 0.074 mm.

2.2 Methods

The HPOH ore was thoroughly mixed with additive, and then pelletized with an appropriate amount of water in a disc pelletizer (d0.8 m×0.2 m) to prepare green pellets of 12 − 16 mm in diameter. Subsequently, the green pellets were dried at 110 °C for 4 h until all free water was removed. The detailed procedure of reduction and magnetic separation tests has already been outlined in an earlier publication [26]. The indexes contain the grade of iron and phosphorus in the magnetic concentrate, iron and phosphorus recovery of the flowsheet, and the metallization of reduced pellets, which are calculated as the follows:

Iron metallization degree of reduced pellets,

$$\eta_{Fe} = \frac{MFe}{TFe} \times 100\% \quad (1)$$

where η_{Fe} is the iron metallization degree of reduced pellets; MFe and TFe are the metallic iron grade and the total iron grade of the reduced pellets, respectively.

Iron (or phosphorus) recovery of the flowsheet,

$$\varepsilon = \frac{w_1}{w_0} \times y \times 100\% \quad (2)$$

where ε is the recovery of iron or phosphorus; w_0 and w_1 are the iron (or phosphorus) content of dry pellets and magnetic separation concentrate, respectively; y is the yield of magnetic separation concentrate.

2.3 Test analysis

X-ray fluorescence spectroscope (XRF) was used to measure the chemical constitutes of the iron ore and the magnetic separation concentrate. Chemical analysis was used to measure the mineral compositions and elemental distribution characteristics of iron and phosphorus in iron ore [31, 32]. X-ray diffractometer (XRD) was used to determine the phase composition of raw ore. Scanning electron microscope (SEM) and an EDAX32 genesis spectrometer (EDS) were used to observe the microstructure of raw ore and reduced pellets. FactSage 7.0 was used to calculate the relationships of standard Gibbs free energy and reaction temperature for the possible reactions.

3 Results and discussion

3.1 Thermodynamic analysis

In this paper, the apatite belongs to fluorapatite and the most reduction reactions of fluorapatite in the absence or presence of SiO_2 and Na_2SO_4 are also studied. Eqs. (3)−(8) are the possible reactions during the direct reduction process, and the result is presented in Figure 4. According to the thermodynamic calculation, fluorapatite is difficult to be reduced by CO (Eq. (3)). However, in the presence of SiO_2 and Na_2SO_4, the Gibbs free energy required for fluorapatite reduction is decreased (Eqs. (4)−(6)). Meanwhile, FeO also can promote the fluorapatite reduction (Eqs. (7) and (8)).

$$2Ca_5(PO_4)_3F + 15CO(g) = 9CaO + CaF_2 + 3P_2(g) + 15CO_2(g) \quad (3)$$

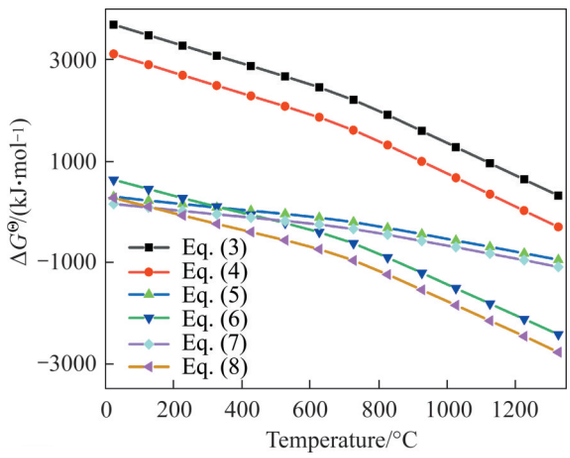

Figure 4 Standard Gibbs free energy change of Eqs. (3)−(8)

$$2Ca_5(PO_4)_3F + 4.5SiO_2 + 15CO(g) = 4.5(2CaO \cdot SiO_2) + CaF_2 + 3P_2(g) + 15CO_2(g) \quad (4)$$

$$Ca_5(PO_4)_3F + 2Na_2SO_4 + 8CO(g) = 3CaNaPO_4 + NaF + 2CaS + 8CO_2(g) \quad (5)$$

$$Ca_5(PO_4)_3F + 5Na_2SO_4 + 20CO(g) = 3Na_3PO_4 + NaF + 5CaS + 20CO_2(g) \quad (6)$$

$$Ca_5(PO_4)_3F + 2Na_2SO4 + 2SiO_2 + 2FeO + 8CO(g) = 3CaNaPO_4 + 2(CaO \cdot SiO_2) + NaF + 2FeS + 8CO_2(g) \quad (7)$$

$$Ca_5(PO_4)_3F + 5Na_2SO_4 + 5SiO_2 + 5FeO + 20CO(g) = 3Na_3PO_4 + 5(CaO \cdot SiO_2) + NaF + 5FeS + 20CO_2 \quad (8)$$

3.2 Direct reduction-magnetic separation

3.2.1 Effect of reduction parameters

Figure 5 presents the effect of reduction parameters on the recovery of phosphorus and iron from the iron ore. When the reduction temperature rises from 1000 to 1150 °C, the recovery rate of iron increases from 87.49% to 93.09%, while that of phosphorus increases from 58.23% to 66.51%. The contents of iron and phosphorus increase from 67.58% to 91.76%, and 1.25% to 1.92%, respectively. Meanwhile, the metallization rate increases from 83.00% to 86.91%. When the temperature exceeds 1150 °C, the recovery of iron and phosphorus changes slightly. Increasing reduction temperature not only can promote the boudouard reaction ($C+CO_2=2CO$), but also promote the reduction of hematite and apatite. The

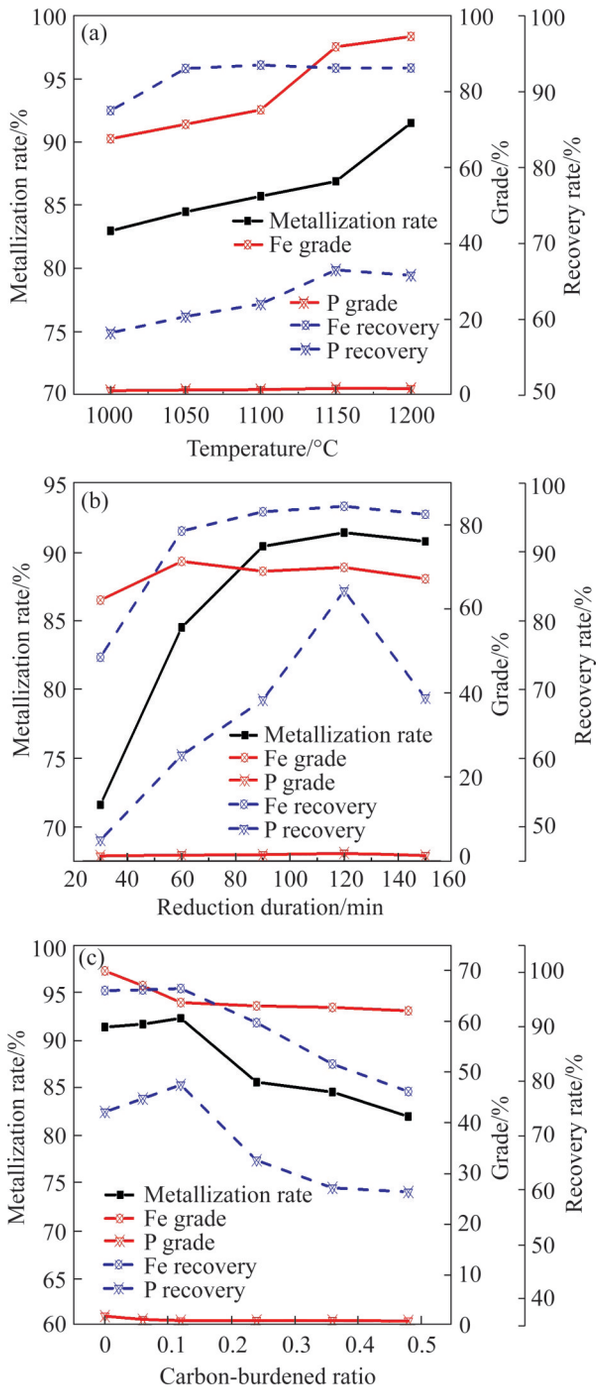

Figure 5 Effect of reduction parameters on recovery of Fe and P from iron ore: (a) Reducing for 60 min with a C/Fe molar ratio of 8.5; (b) Reducing at 1050 °C with a C/Fe molar ratio of 8.5; (c) Reducing at 1050 °C for 120 min with a Total C/Fe molar ratio of 8.5

appearance of reduced pellets obtained at 1050 and 1100 °C is presented in Figure 6. It can be seen that there is much liquid iron precipitate on the contact surfaces of the pellets at 1100 °C. Because of the raw ore contains a high content of silicon and

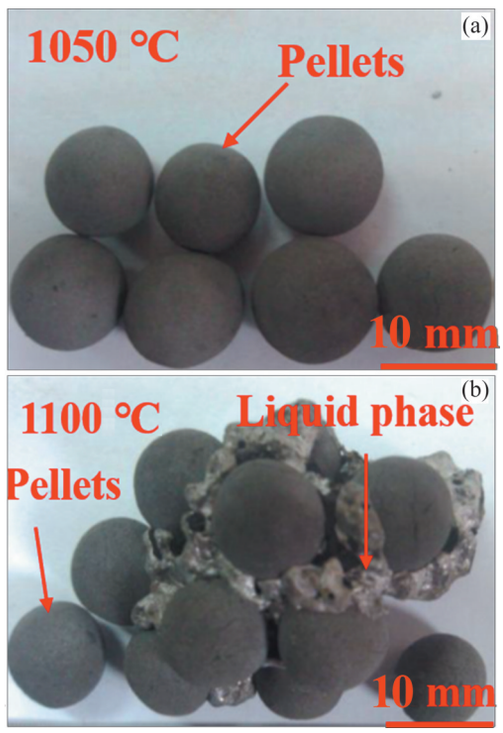

Figure 6 Appearance of reduced pellets (a) and pellets with liquid phase (b)

aluminum, a low melting point material is formed. Further elevating the reduction temperature, the reduced pellets will melt. In consideration of the practical application, 1050 °C was recommended as the appropriate reduction temperature.

Under the conditions of reducing at 1050 °C with a C/Fe mole ratio of 8.5, five reduction duration of 30, 60, 90, 120 and 150 min were chosen to investigate the effects on the phosphorus and iron recovery, and the results are shown in Figure 5(b). It is known that the iron and phosphorus recoveries improve significantly by extending the reduction duration from 30 to 120 min. Extending the reduction duration to 150 min has a negative impact on the indexes. Consequently, the reduction atmosphere was weakened, leading to the re-oxidation of the metallic iron. When part of the phosphorus from apatite transfers into the concentrate, some may get lost due to volatilization of gaseous P_2 [2]. Meanwhile, the metallization rate increases from 71.58% to 91.40% with prolonging the reduction duration from 30 to 120 min. Overall, 120 min is considered sufficient for the iron and phosphorus recovery. In this case, magnetic concentrate with

69.95% iron and 1.92% phosphorus at recovery rates of 96.65% and 74.34%, respectively, can be obtained.

The carbon-burdened is widely used to improve the reduction of complex iron ore [33, 34]. Different carbon-burdened ratios were investigated to reveal the effect of carbon-burdened ratio on the recovery of iron and phosphorus, and the results are shown in Figure 5(c). The grade of iron and phosphorus decreaseds with the increase of carbon-burdened ratio from 0 to 0.48. Meanwhile, the metallization rate, the recovery of iron and phosphorus increases with increasing carbon-burdened ratio from 0 to 0.12. Further elevating the ratio has a negative impact because excessive coal can cause carburization and bring more impurity from coal ash.

The microstructure of the reduced pellets obtained without and with a carbon-burdened ratio of 0.12 is presented in Figure 7. As can be seen, there is no difference between the internal and outer structure of reduced pellets obtained without carbon-burdened. Metallic iron mainly distributes among the oolitic. Compared with no carbon-burdened, there is difference between the internal and outer structure of reduced pellets obtained with carbon-burdened. The outer structure of reduced pellets is the same as that without carbon-burden, and the iron oxides are not reduced completely. However, the iron oxides are reduced sufficient internal of reduced pellets, and the iron grains aggregate and grow.

The SEM-EDS analyses of the reduced pellets with a 0.12 coal-bearing mole ratio are shown in Figure 8, and the element contents of points 1−4 are presented in Table 5. According to the thermodynamic analysis, the solubility of phosphorus in α-Fe at 1050 °C is 2.8%, and the metallic iron contains a small amount of phosphorus (Point 1), which consists with the thermodynamics analysis. Most of apatite is not reduced, and it distributes with gangue (Points 2 and 3). The metallic iron particle close to the apatite is likely to form a solid solution of Fe-P, while the metallic iron far from the apatite particle is pure (Point 4). The reduction of the scattered apatite is the crucial and major reason responsible for the formation of Fe-P alloy.

3.2.2 Effect of Na_2SO_4 dosage

Figure 9 shows the effect of Na_2SO_4 dosage on the iron and phosphorus recovery. The recovery of iron and phosphorus decreases from 97.04% to 95.43% and 79.32% to 68.99%, respectively with increasing the Na_2SO_4 dosage from 0% to 15%.

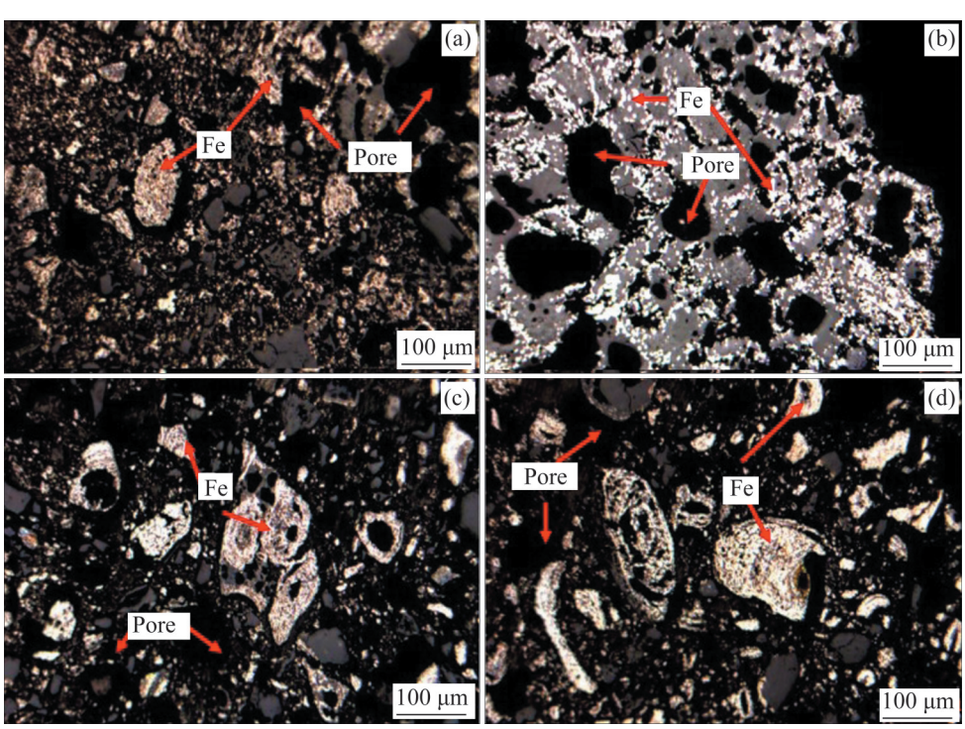

Figure 7 Microstructure of reduced pellets: (a) Outer and (b) inner layer with carbon-burdened ratio of 0.12; (c) Outer and (d) inner layer without carbon-burdened

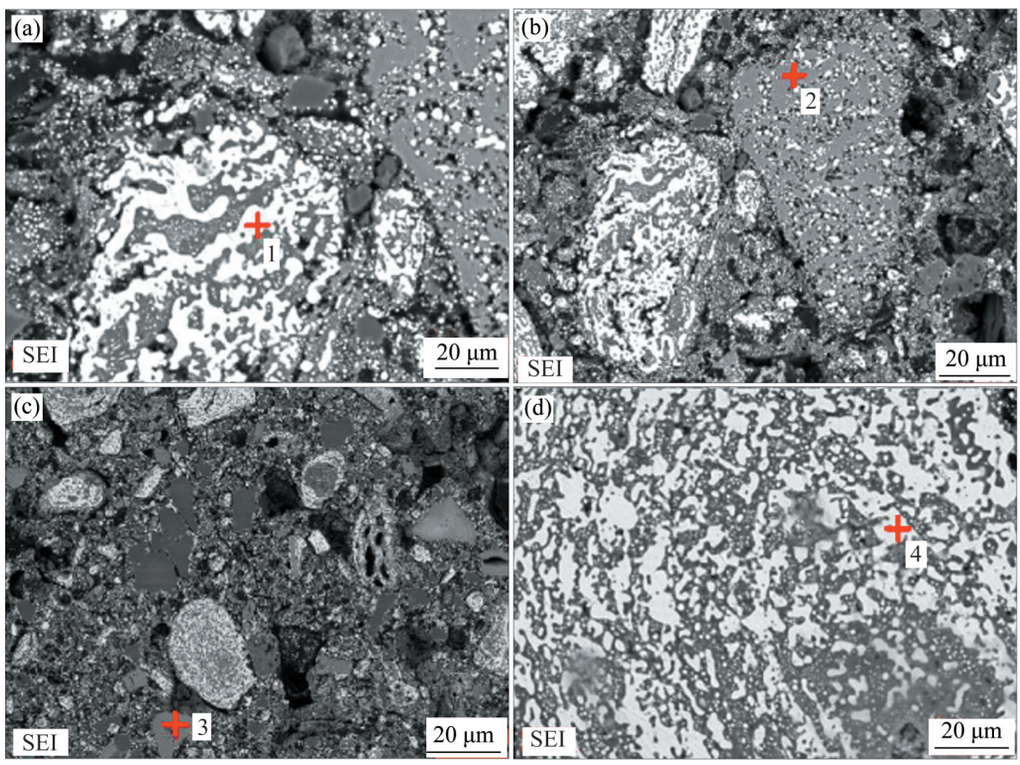

Figure 8 SEM images of major phases in reduced pellets: (a) P-bearing metallic iron; (b) Slag phase; (c) Residual apatite; (d) Metallic iron

Table 5 Composition (wt%) of points 1−4

Point	OK	SiK	PK	CaK	FeK
1	–	–	1.24	–	98.76
2	28.26	16.83	18.46	36.44	–
3	34.97	–	23.51	41.51	–
4	–	–	–	–	100

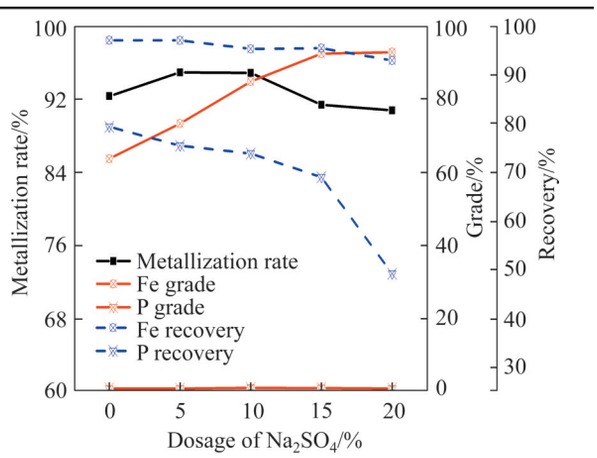

Figure 9 Effect of Na_2SO_4 dosage on recovery of iron and phosphorus (Reducing at 1050 °C for 120 min with a Total C/Fe (mole ratio) of 8.5, carbon-burdened ratio of 0.12 in pellets)

However, the iron content of the concentrate increases from 63.71% to 92.40%. Meanwhile, the content of phosphorus maintains about 1%. when increasing the Na_2SO_4 dosage from 0% to 10%, the metallization rate of reduced pellets is raised from 92.33% to 98.87%. Further increasing the dosage, the metallization rate decreases because of the formation of FeS. Adding Na_2SO_4 has a positive impact on the growth of iron grain, which increases the iron content of concentrate [22]. However, it inhibits the reduction of apatite, causing most of apatite is not reduced and enters into the non-magnetic tailing, thereby reducing the phosphorus recovery. From above, 15% was recommended as the optimal Na_2SO_4 dosage.

The microstructure of reduced pellets is shown in Figure 10. The metallic iron area of the edge and central of pellet increases obviously, and the iron grain size increases to more than 20 μm. Meanwhile, there are many hole structures. The boundary between the metallic iron grain and gangue is obvious, and a large amount of FeS generates in the center of pellet. The SEM-EDS of reduced pellets is presented in Figure 11, and the composition of Points 1−3 is presented in Table 6. The bright areas are Fe-P alloy with a phosphorus

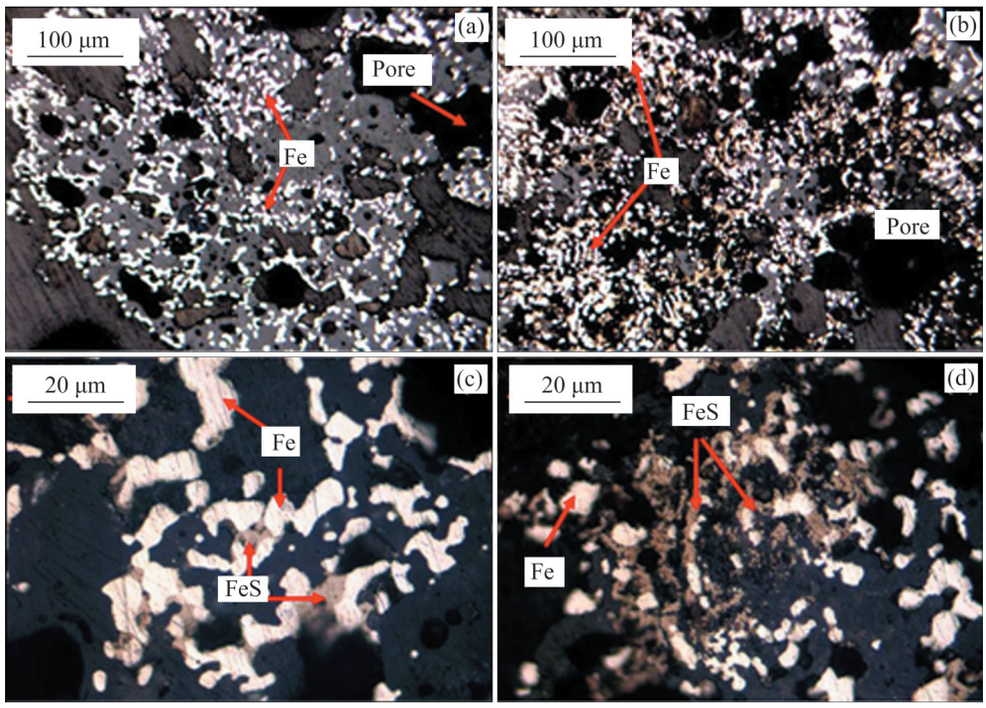

Figure 10 Microstructure of reduced pellets with addition of 15% Na_2SO_4: (a, c) Outer layer; (b, d) Inner layer

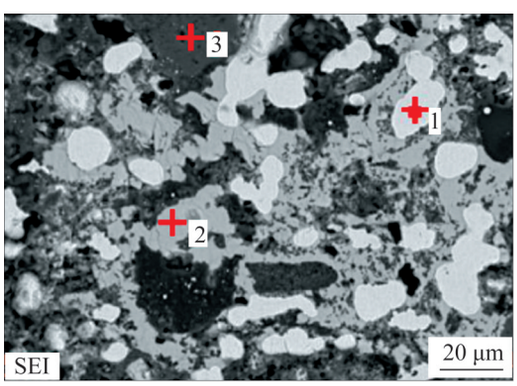

Figure 11 SEM image of main phases in reduced pellets

Table 6 Element content (wt%) of points 1−3

Point	O	Na	Al	Si	P	S	Ca	Mn	Fe
1	–	–	–	–	1.19	–	–	–	98.81
2	–	–	–	–	–	39.01	–	1.56	59.43
3	28.90	2.22	2.22	3.32	21.30	0.91	41.91	–	–

content of 1.19% (Point 1), and the light gray areas are FeS (Point 2). A small amount of sodium aluminosilicate is embedded in apatite (Point 3). A large amount of FeS generates in the reduced pellets, which can provide a liquid phase bridge for the aggregation of iron grains and promote the growth of iron grains. However, it is difficult to be reduced and it has a negative impact on the metallization rate.

The L_P decreases with increasing Na_2SO_4 dosage, which means that the content of phosphorus in metal phase is decreased, thus the phosphorus recovery decreases. The result is consistent with the experimental phenomenon.

3.2.3 Optimization of magnetic separation parameters

The effect of magnetic separation parameters on the recovery of Fe and P is shown in Figure 12. The recovery rate of iron and phosphorus increased from 92.08% to 95.43%, and 66.69% to 68.99%, respectively, when the magnetic field intensity increases from 44.65 to 74.41 kA/m. However, the iron and phosphorus recovery changes slightly with increasing magnetic field intensity. This is because most of the apatite has not been reduced and entered the gangue during magnetic separation.

Figure 12(b) presents the effect of grinding fineness (<0.074 mm) on the indexes of the reduction process. The iron grade increases from 64.97% to 92.40% with the increase of grinding fineness (<0.074 mm) from 90.50% to 98.65%. The grade and recovery of phosphorus decrease from 1.35% to 1.09%, and 77.74% to 68.99%, respectively. This is because most phosphorus in the reduced pellets did not form a solid solution with

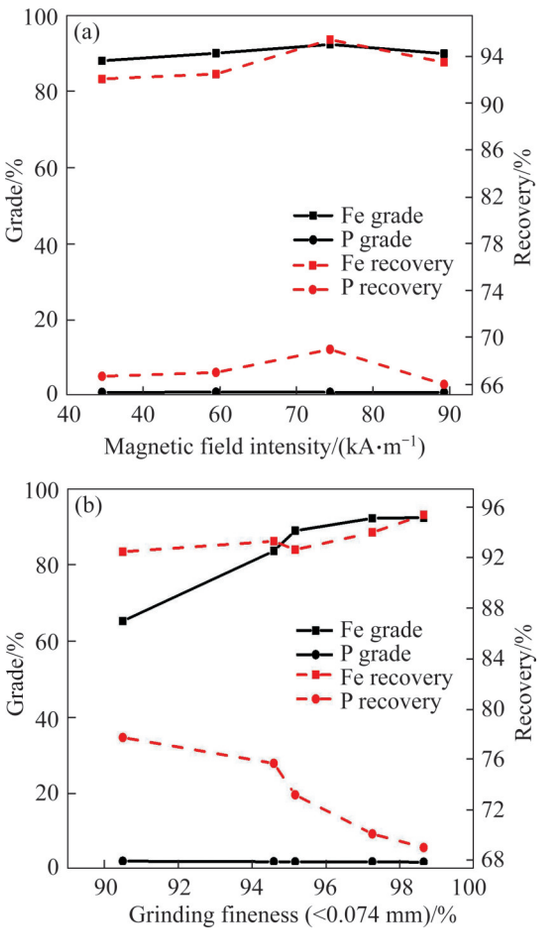

Figure 12 Effect of magnetic separation parameters on recovery of iron and phosphorus: (a) Magnetic field intensity; (b) Grinding fineness

metallic iron, but still existed in the form of apatite, which can be removed through magnetic separation into non-magnetic fraction.

From above, the optimal conditions are presented: reduction at 1050 °C for 120 min with a C/Fe mole ratio of 8.5, carbon-burdened ratio of 0.12 in the pellets with 15% Na_2SO_4 and grinding the reduced ore to 98.65% is in size <0.074 mm at magnetic field intensity of 74.41 kA/m. The Fe-P alloy assaying 92.40% Fe_{total} and 1.09% P is achieved at an overall iron recovery of 95.43% and phosphorus recovery of 68.98%, respectively, which could be used as the burden for weathering resistant steel, and the non-magnetic tailings can be applied as building materials [35].

4 Conclusions

High-phosphorus oolitic hematite ore, containing 41.50% Fe_{total} and 1.24% P, is used as a raw material to prepare Fe-P alloy using the direct reduction-magnetic separation process. Under the conditions of 15% Na_2SO_4 and carbon-burdened ratio of 0.12, reducing at 1050 °C for 120 min with a total C/Fe (molar ratio) of 8.5, the final product, containing 92.40% Fe and 1.09% P is achieved at an overall iron recovery of 95.43% and phosphorus recovery of 68.98%, respectively. This metallized Fe-P powder can be applied as the burden for production of weathering resistant steels. The mechanism study reveals that part of apatite is reduced to P_2 gas, and then the generated P_2 can dissolve into metallic iron to form Fe-P solid solution.

Contributors

LI Si-wei performed the data analysis and wrote the manuscript. PAN Jian and ZHU De-qing obtained the project. GUO Zheng-qi and YANG Cong-cong contributed to the methodology. LI Si-wei, DONG Tao and LU Sheng-hu conducted experimental tests. All authors replied to reviewer' comments and revised the final version.

Conflict of interest

LI Si-wei, PAN Jian, ZHU De-qing, YANG Cong-cong, GUO Zheng-qi, DONG Tao, and LU Sheng-hu declare that they have no conflict of interest.

References

[1] MORCILLO M, DIAZ I, CANO H, CHICO B, FUENTE D. Atmospheric corrosion of weathering steels. Overview for engineers. Part I: Basic concepts [J]. Construction and Building Materials, 2019, 213: 723 – 737. DOI: 10.1016/j.conbuildmat.2019.03.334.

[2] SAHOO G, SINGH B, SAXENA A. Characterization of high phosphorous containing hot rolled weather resistant structural steels [J]. Materials Science and Engineering, 2015, 628: 303–310. DOI: 10.1016/j.msea.2015.01.059.

[3] GUO Zheng-qi, ZHU De-qing, PAN Jian, ZHANG Feng. Innovative methodology for comprehensive and harmless utilization of waste copper slag via selective reduction-magnetic separation process [J]. Journal of Cleaner Production, 2018, 187: 910 – 922. DOI: 10.1016/j. jclepro.2018.03.264.

[4] MORCILLO M, DIAZ I, CHICO B, CANO H, FUENTE D. Weathering steels: From empirical development to scientific design – A review [J]. Corrosion Science, 2014, 83: 6 – 31.

DOI: 10.1016/j.corsci.2014.03.006.

[5] ZHOU G P, LIU Z Y, QIU Y Q, WANG G D. The improvement of weathering resistance by increasing P contents in cast strips of low carbon steels [J]. Materials and Design, 2009, 30(10): 4342 – 4347. DOI: 10.1016/j. matdes. 2009.04.010.

[6] MORCILLO M, CHICO B, DIAZ I, CANO H, FUENTE D. Atmospheric corrosion data of weathering steels – A review [J]. Corrosion Science, 2013, 77: 6 – 24. DOI: 10.1016/j. corsci.2013.08.021.

[7] KEITH Q. A review on the characterization and processing of oolitic iron ores [J]. Minerals Engineering, 2018, 126: 89–100. DOI: 10.1016/j.mineng.2018.06.018.

[8] SONG Shao-xian, FABIN C T, ZHANG Yi-min, LOPEZ-VALDIVIESO A. Morphological and mineralogical characterizations of oolitic iron ore in the Exi region, China [J]. International Journal of Minerals Metallurgy and Materials, 2013, 20(2): 113–118. DOI: 10.1007/s12613-013-0701-z.

[9] XIAO Jun-hui, ZOU Kai, WANG Zhen. Studying on mineralogical characteristics of a refractory high-phosphorous oolitic iron ore [J]. SN Applied Sciences, 2020, 2: 1051–1062. DOI: 10.1007/s42452-020-2871-4.

[10] ZHANG Long, MACHIELA R, ZHANG Ming-ming, EISELE T. Dephosphorization of unroasted oolitic ores through alkaline leaching at low temperature [J]. Hydrometallurgy, 2019, 184: 95 –102. DOI: 10.1016/j. hydromet.2018.12.023.

[11] ZHU De-qing, ZHOU Xian-lin, PAN Jian, LUO Yan-hong. Direct reduction and beneficiation of a refractory siderite lump [J]. Mineral Processing Extraction Metallurgy, 2014, 123(4): 246–250. DOI: 10.1179/1743285514y.0000000081.

[12] CHUN Tie-jun, LONG Hong-ming, LI Jia-xin. Alumina-iron separation of high alumina iron ore by carbothermic reduction and magnetic separation [J]. Separation Science and Technology, 2015, 50(5): 760 – 766. DOI: 10.1080/01496395.2014.959601.

[13] LI Si-wei, PAN Jian, ZHU De-qing, GUO Zheng-qi, SHI Yue, CHOU Jian-lei, XU Ji-wei. An innovative technique for comprehensive utilization of high aluminum iron ore via pre-reduced-smelting separation-alkaline leaching process: Part I: Pre-reduced-smelting separation to recover iron [J]. Metals, 2020, 10: 57. DOI: org/10.3390/met10010057.

[14] ZHOU Xian-lin, ZHU De-qing, PAN Jian, LUO Yan-hong, LIU Xin-qi. Upgrading of high-aluminum hematite-limonite ore by high temperature reduction-wet magnetic separation process [J]. Metals, 2016, 6: 57 – 69. DOI: 10.3390/met603 0057.

[15] BAO Qi-peng, GUO Lei, GUO Zhan-cheng. A novel direct reduction-flash smelting separation process of treating high phosphorous iron ore fines [J]. Powder Technology, 2021, 377: 149–162. DOI: 10.1016/j.powtec.2020.08.066.

[16] ZHOU Wen-tao, HAN Yue-xin, SUN Yong-sheng, LI Yan-jun. Strengthening iron enrichment and dephosphorization of high-phosphorus oolitic hematite using high-temperature pretreatment [J]. International Journal of Minerals, Metallurgy and Materials, 2020, 27: 443–453. DOI: 10.1007/s12613-019-1897-3.

[17] YU Wen, SUN Ti-chang. Can sodium sulfate be used as an additive for the reduction roasting of high-phosphorus oolitic hematite ore? [J]. International Journal of Mineral Processing, 2014, 133: 119 – 122. DOI: 10.1016/j. minpro. 2014.10.008.

[18] TANG Hui-qing, GUO Zhan-cheng, ZHAO Zhi-long. Phosphorus removal of high phosphorus iron ore by gas-based reduction and melt separation [J]. Journal of Iron and Steel Research International, 2010, 17(9): 1–6. DOI: 10.1016/S1006-706X(10)60133-1.

[19] SUN Yong-sheng, LI Yan-feng, HAN Yue-xin, LI Yan-jun. Migration behaviors and kinetics of phosphorus during coal-based reduction of high-phosphorus oolitic iron ore [J]. International Journal of Minerals, Metallurgy and Materials, 2019, 26: 938–945. DOI: 10.1007/s12613-019-1810-0.

[20] MATINDE E, HINO M. Dephosphorization treatment of high phosphorus iron ore by pre-reduction, mechanical crushing and screening methods [J]. ISIJ International, 2011, 51(2): 220–227. DOI: 10.2355/isijinternational.51.220.

[21] TANG Hui-qing, LIU Wei-di, ZHANG Huan-yu, GUO Zhan-cheng. Effect of microwave treatment upon processing oolitic high phosphorus iron ore for phosphorus removal [J]. Metallurgical and Materials Transactions B, 2014, 45(5): 1683–1694. DOI: 10.1007/s11663-014-0072-5.

[22] CHENG C Y, MISRA V N, CLOUGH J, MUN R. Dephosphorization of Western Australian iron ore by hydrometallurgical process [J]. Minerals Engineering, 1999, 12: 1083–1092. DOI: 10.1016/S0892-6875(99)00093-X.

[23] RAO Ming-jun, OUYANG Chong-zhong, LI Guang-hui, ZHANG Shu-hui, ZHANG Yuan-bo, JIANG Tao. Behavior of phosphorus during the carbothermic reduction of phosphorus-rich oolitic hematite ore in the presence of Na_2SO_4 [J]. International Journal of Mineral Processing, 2015, 143: 72–79. DOI: 10.1016/j.minpro.2015.09.002.

[24] ZHU De-qing, CHUN Tie-jun, PAN Jian, LU Li-ming, HE Zhen. Upgrading and dephosphorization of western Australian iron ore using reduction roasting by adding sodium carbonate [J]. International Journal of Minerals Metallurgy and Materials, 2013, 20: 505–513. DOI: 10.1007/s12613-013-0758-8.

[25] ZHU De-qing, GUO Zheng-qi, PAN Jian, ZHANG Feng. Synchronous upgrading iron and phosphorus removal from high phosphorus oolitic hematite ore by high temperature flash reduction [J]. Metals, 2016, 6: 123–139. DOI: 10.3390/met6060123.

[26] YANG Cong-cong, ZHU De-qing, PAN Jian, LU Li-ming. Simultaneous recovery of iron and phosphorus from a high-phosphorus oolitic iron ore to prepare Fe-P Alloy for high-phosphorus steel production [J]. JOM, 2017, 69: 1663–1668. DOI: 10.1007/s11837-017-2385-8.

[27] SUN Yong-sheng, ZHANG Qi, HAN Yue-xin, GAO Peng, LI Guo-feng. Comprehensive utilization of iron and phosphorus from high-phosphorus refractory iron ore [J]. JOM, 2018, 70: 144–149. DOI: 10.1007/s11837-017-2637-7.

[28] HAN Yue-xin, LI Yan-feng, GAO Peng, SUN Yong-sheng. Reduction behavior of apatite in oolitic hematite ore using coal as a reductant [J]. Ironmaking and Steelmaking, 2017, 44: 287–296. DOI: 10.1080/03019233.2016.1210750.

[29] SONG Yong-sheng, HAN Yue-xin, GAO Peng, WANG Qin. Effect of temperature on coal-based reduction of an oolitic

iron ore [J]. Journal of China University of Mining &Technology, 2015, 44(1): 132−137. (in Chinese).

[30] LI Si-wei, PAN Jian, ZHU De-qing, GUO Zheng-qi, XU Ji-wei, CHOU Jian-lei. A novel process to upgrade the copper slag by direct reduction-magnetic separation with the addition of Na_2CO_3 and CaO [J]. Powder Technology, 2019, 347: 159−169. DOI: 10.1016/j.powtec.2019.02.046.

[31] XU Yan, SUN Ti-chang, LIU Zhi-guo, XU Cheng-yan. Phosphorus occurrence state and phosphorus removal research of a high phosphorus oolitic hematite by direct reduction roasting method [J]. Journal of Northeastern University, 2013, 34(11): 1651−1655. (in Chinese)

[32] ZHAO Ren, YIN Lin, ZHAO Lian-ze, XIONG Fei. Research on the occurrence of Fe in sericite, Chuzhou, Anhui Province, Southeast China [J]. Acta Mineralogical Sinica, 2004, 24: 309−314. (in Chinese)

[33] WEI Yu-xia, SUN Ti-chang, KOU Jue, YU Wen, CAO Yun-ye. Effect of coal dosage on direct reduction roasting of refractory iron ore briquettes [J]. Journal of Central South University (Science and Technology), 2013, 44(4): 1305 − 1311. (in Chinese)

[34] LU W K, HUANG D F. The evolution of ironmaking process based on coal-containing iron ore agglomerates [J]. ISIJ International, 2001, 41(8): 807 − 812. DOI: 10.2355/isijinternational.41.807.

[35] LIU Qiang, PAN Zhi-hua, LI Qing-bin, RUAN Yu-hua. Preparation of anorthite lightweight thermal insulating brick and the formation process of anorthite [J]. Bulletin Chinese Ceram Soc, 2010, 29: 1269−1274. (in Chinese)

(Edited by FANG Jing-hua)

中文导读

采用直接还原-磁选工艺从高磷鲕状赤铁矿中同步富集铁和磷制备Fe-P合金

摘要：本文采用直接还原-磁选工艺从高磷鲕状赤铁矿中同步富集铁和磷制备Fe-P合金。结果表明，在低温和无添加剂情况下，由于鲕状结构未破坏导致铁不能被有效回收。在还原温度为1050 °C，还原时间为120 min，总碳/铁(物质的量比)为8.5，Na_2SO_4添加量为15%的条件下得到的Fe-P合金中铁品位为92.40%，磷品位为1.09%，两者的回收率分别为95.43%和68.98%。所得到的Fe-P金属粉末可用作耐候钢的生产原料。此工艺可以有效和绿色地利用高磷鲕状赤铁矿。

关键词：高磷鲕状赤铁矿；直接还原；磁选；Fe-P合金